

A Boundary Perturbation Method for Vector Electromagnetic Scattering from Families of Doubly Periodic Gratings

David P. Nicholls · Joseph Orville

Received: 15 June 2009 / Revised: 23 October 2009 / Accepted: 15 January 2010 /
Published online: 27 January 2010
© Springer Science+Business Media, LLC 2010

Abstract In this paper the authors extend their previous work on Boundary Perturbation methods for scattering calculations from families of diffraction gratings to three dimensions and the full vector electromagnetic Maxwell equations. This extension is non-trivial in both its algorithmic implementation (not only are new terms added to the recursions, but also the full, coupled, vector Maxwell equations must be simulated) and in the size of the relevant computer simulations. Not only do we give details of the implementation of the method, but also provide results of numerical simulations.

Keywords Electromagnetic scattering · Boundary Perturbation methods · High-order spectral methods · Traveling water waves

1 Introduction

The scattering of electromagnetic radiation by irregular obstacles and rough surfaces plays a crucial role in a wide array of applications of engineering interest including remote sensing, non-destructive testing, and radar imaging. Of particular interest to us here is the interaction of this radiation with the surface of a traveling open-ocean wave modeled by the “water wave equations” [5]. Such waves are known to be parametrized analytically by a height/slope parameter [10, 14] and in this work we use this fact to design a numerical scheme to compute scattering quantities of interest for the *entire* family of possible solutions *simultaneously* thereby constituting a highly efficient method for recovering these measurements as compared to other state-of-the-art solvers which must compute with one profile at a time [15]. In this contribution we focus on the case of a perfectly conducting (PEC) family of gratings and leave the more complicated case of dielectrics for future work.

This work generalizes the recent contribution of one of the authors [6] from the case of the scattering of acoustic waves in two dimensions by a rough interface (governed by

D.P. Nicholls (✉) · J. Orville
Department of Mathematics, Statistics, and Computer Science, University of Illinois at Chicago,
Chicago, IL 60607, USA
e-mail: nicholls@math.uic.edu

the scalar Helmholtz equation), to not only three dimensions, but also the full vector electromagnetic Maxwell equations. Each of these generalizations provides its own set of new challenges including vast new memory and computational time requirements, and the need to deal with the vector Helmholtz equations coupled by the surface boundary conditions. As we shall show, the rapid execution time that can be achieved with this new method is due to the phase extraction we perform (which greatly simplifies the boundary conditions), and the change of independent variables which moves the boundary dependence of the problem from the domain definition to the inhomogeneities of the governing Helmholtz equation and boundary conditions. Finally, a Boundary Perturbation algorithm, resulting in a high-order Fourier collocation/Chebyshev tau/Taylor method, is applied resulting in a highly accurate and robust computational approach. This change of variables coupled to a Boundary Perturbation approach (the method of “Transformed Field Expansions”—TFE) has been utilized in a number of contexts recently, including Laplace’s equation [7], the scalar Helmholtz equation [6, 9], and the classical water wave problem [10] with great success. As we find later, this success is reproduced here resulting in a compelling algorithm for the scenario we describe.

The paper is organized as follows: In Sect. 2 we recall the governing equations of vector electromagnetics in three dimensions. In Sects. 2.1 and 2.2 we detail the phase extraction and domain flattening changes of variables crucial to our approach, and in Sects. 2.3 and 2.4 we outline the TFE recursions in this new vector electromagnetic setting and the generalizations necessary to make this method applicable to families of gratings. In Sect. 3 we present numerical results including verification of our new scheme and plots of grating efficiencies. In Sect. 4 we make concluding remarks.

2 Governing Equations

Time-harmonic vector electromagnetic radiation (characterized by the electric and magnetic fields \mathbf{E} and \mathbf{H} , respectively) in three dimensions incident upon a perfectly conducting grating shaped by the smooth function $z = g(x, y)$ satisfies Maxwell’s equations

$$\nabla \times \mathbf{E} = ik\mathbf{H} \quad z > g(x, y), \quad (2.1a)$$

$$\nabla \times \mathbf{H} = -ik\mathbf{E} \quad z > g(x, y), \quad (2.1b)$$

$$\operatorname{div}[\mathbf{E}] = 0 \quad z > g(x, y), \quad (2.1c)$$

$$\operatorname{div}[\mathbf{H}] = 0 \quad z > g(x, y), \quad (2.1d)$$

$$\mathbf{n} \times \mathbf{E} = -\mathbf{n} \times \mathbf{E}^i \quad z = g(x, y), \quad (2.1e)$$

where the incident field is given by

$$\mathbf{E}^i = \mathbf{A}e^{i\mathbf{k}\cdot\mathbf{x}} = \mathbf{A}e^{i(\alpha x + \beta y - \gamma z)}, \quad \mathbf{H}^i = \mathbf{B}e^{i\mathbf{k}\cdot\mathbf{x}} = \mathbf{B}e^{i(\alpha x + \beta y - \gamma z)},$$

$$\mathbf{k} = (\alpha, \beta, -\gamma), \quad k = |\mathbf{k}|, \quad \mathbf{B} = \frac{\mathbf{k}}{|\mathbf{k}|} \times \mathbf{A}, \quad \mathbf{A} \cdot \mathbf{k} = 0.$$

Later it will be convenient to express vector quantities componentwise, e.g., $\mathbf{E} = (E^1, E^2, E^3)$, $\mathbf{A} = (A^1, A^2, A^3)$, etc. Clearly, once the electric field \mathbf{E} has been found, the magnetic field can be recovered trivially from (2.1a) and thus we focus on simulating the

former. Through well-known manipulations of (2.1) (see, e.g., [15]), the governing equation for the electric field can be reduced to the vector Helmholtz equation

$$\Delta \mathbf{E} + k^2 \mathbf{E} = 0, \quad z > g(x, y). \tag{2.2}$$

To realize a unique solution, this equation is supplemented with boundary conditions, one of which is the “outgoing wave condition” which states that scattered waves propagate away from the grating. For the case of a bi-periodic grating which we consider here

$$g(x + d_1, y, z) = g(x, y, z), \quad g(x, y + d_2, z) = g(x, y, z),$$

this condition at infinity can be stated rigorously in the near-field (at $z = a$, $a > |g|_{L^\infty}$) by means of the Rayleigh expansion [6]:

$$\partial_z \mathbf{E} - (i\gamma_D) \mathbf{E} = 0, \quad z = a. \tag{2.3}$$

Here $(i\gamma_D)$ is a Fourier multiplier of order one defined by

$$(i\gamma_D)\psi(x, y) := \sum_{p=-\infty}^{\infty} \sum_{q=-\infty}^{\infty} (i\gamma_{p,q}) \hat{\psi}_{p,q} e^{i(\alpha_p x + \beta_q y)},$$

where,

$$\hat{\psi}_{p,q} = \frac{1}{d_1 d_2} \int_0^{d_1} \int_0^{d_2} \psi(x, y) e^{i(\alpha_p x + \beta_q y)} dx dy.$$

In these equations

$$\alpha_p := \alpha + (2\pi/d_1)p, \quad \beta_q := \beta + (2\pi/d_2)q,$$

$$\gamma_{p,q} := \begin{cases} \sqrt{k^2 - \alpha_p^2 - \beta_q^2} & (p, q) \in U, \\ i\sqrt{\alpha_p^2 + \beta_q^2 - k^2} & (p, q) \notin U, \end{cases}$$

and

$$U := \{(p, q) \in \mathbf{Z}^2 \mid k^2 - \alpha_p^2 - \beta_q^2 \geq 0\},$$

is the set of propagating modes. Finally, we have the surface boundary condition, (2.1e), which we rewrite, to simplify our later developments, by using the normal vector

$$\mathbf{N} = (-\partial_x g, -\partial_y g, 1)^T$$

resulting in:

$$\mathbf{N} \times \mathbf{E} = -\mathbf{N} \times \mathbf{E}^i = -(\mathbf{N} \times \mathbf{A}) e^{i(\alpha x + \beta y - \gamma g(x, y))}. \tag{2.4}$$

This can be written componentwise as

$$\begin{aligned} -E^2 - (\partial_y g) E^3 &= -\{ -A^2 - (\partial_y g) A^3 \} e^{i(\alpha x + \beta y - \gamma g(x, y))}, \\ E^1 + (\partial_x g) E^3 &= -\{ A^1 + (\partial_x g) A^3 \} e^{i(\alpha x + \beta y - \gamma g(x, y))}, \\ (\partial_y g) E^1 - (\partial_x g) E^2 &= -\{ (\partial_y g) A^1 - (\partial_x g) A^2 \} e^{i(\alpha x + \beta y - \gamma g(x, y))}. \end{aligned}$$

Keeping only the first two (as the third is a linear combination of these), reordering, and simplifying:

$$E^1 = -A^1 e^{i(\alpha x + \beta y - \gamma g(x,y))} - (\partial_x g) \{A^3 e^{i(\alpha x + \beta y - \gamma g(x,y))} + E^3\}, \tag{2.5a}$$

$$E^2 = -A^2 e^{i(\alpha x + \beta y - \gamma g(x,y))} - (\partial_y g) \{A^3 e^{i(\alpha x + \beta y - \gamma g(x,y))} + E^3\}. \tag{2.5b}$$

With (2.2), (2.3), and (2.5) we require only one more equation for a properly posed problem. For this we use the divergence-free condition, (2.1c),

$$\partial_x E^1 + \partial_y E^2 + \partial_z E^3 = 0. \tag{2.6}$$

Collecting all of these we find that we must solve the system of vector-valued PDE

$$\Delta \mathbf{E} + k^2 \mathbf{E} = 0 \quad g(x, y) < z < a, \tag{2.7a}$$

$$\partial_z \mathbf{E} - (i\gamma_D) \mathbf{E} = 0 \quad z = a, \tag{2.7b}$$

$$M \mathbf{E} = \Phi(x, y; \mathbf{E}, g) \quad z = g, \tag{2.7c}$$

where

$$M := \begin{pmatrix} 1 & 0 & 0 \\ 0 & 1 & 0 \\ \partial_x & \partial_y & \partial_z \end{pmatrix}, \tag{2.7d}$$

and

$$\Phi := \begin{pmatrix} -A^1 e^{i(\alpha x + \beta y - \gamma g(x,y))} - (\partial_x g) \{A^3 e^{i(\alpha x + \beta y - \gamma g(x,y))} + E^3\} \\ -A^2 e^{i(\alpha x + \beta y - \gamma g(x,y))} - (\partial_y g) \{A^3 e^{i(\alpha x + \beta y - \gamma g(x,y))} + E^3\} \\ 0 \end{pmatrix}. \tag{2.7e}$$

We note that we have organized Φ so that it contains any \mathbf{E} -terms which are $\mathcal{O}(g)$ and thus “higher order corrections” in the boundary perturbation g .

A quantity of considerable importance in applications is the surface current given by

$$\tilde{\mathbf{J}} = \mathbf{n} \times \mathbf{H}, \quad \text{at } z = g,$$

where $\mathbf{n} := \mathbf{N}/|\mathbf{N}|$. Again, for later convenience, we use the normal \mathbf{N} resulting in the rescaled surface current

$$\mathbf{J} = \mathbf{N} \times \mathbf{H}, \quad \text{at } z = g.$$

Using the fact that $\mathbf{H} = 1/(ik)\nabla \times \mathbf{E}$ we have

$$\mathbf{J} = \frac{1}{ik} \mathbf{N} \times (\nabla \times \mathbf{E}), \quad \text{at } z = g.$$

In Cartesian coordinates these read

$$J^1 = \frac{1}{ik} \{ \partial_x E^3 - \partial_z E^1 + (\partial_y g) (\partial_y E^1 - \partial_x E^2) \}, \tag{2.8a}$$

$$J^2 = \frac{1}{ik} \{ \partial_y E^3 - \partial_z E^2 + (\partial_x g) (\partial_x E^2 - \partial_y E^1) \}, \tag{2.8b}$$

$$J^3 = \frac{1}{ik} \{ (\partial_x g) (\partial_x E^3 - \partial_z E^1) + (\partial_y g) (\partial_y E^3 - \partial_z E^2) \}. \tag{2.8c}$$

2.1 Phase Extraction

For our purposes it is convenient to extract the phase from our governing equations by considering the rescaled quantity \mathbf{v} as our unknown from the relationship

$$\mathbf{E} = e^{i(\alpha x + \beta y - \gamma z)} \mathbf{v}. \tag{2.9}$$

This factorization is inspired by the well-known asymptotic result that at high frequencies ($k \gg 1$) and in the absence of shadowing, multiple reflections, etc., the scattered surface current oscillates with the incident radiation. This implies that in this situation (the surface curl of) \mathbf{v} will be *slowly* varying, even for large k , which is an idea we have put into practice in [11] but do not pursue further here as we focus upon the regime $k \approx 1$. For us the advantage of the factorization (2.9) is that while the boundary data for \mathbf{E} at $z = g$ contains somewhat complicated, *explicit*, dependence upon the boundary shape g , the factored boundary data is much simpler and thus more amenable to our techniques.

It is not difficult to show [6] that the change of dependent variable (2.9) transforms the governing equations (2.7) to

$$\Delta \mathbf{v} + 2i(\alpha, \beta, -\gamma) \cdot \nabla \mathbf{v} = 0 \quad g(x, y) < z < a, \tag{2.10a}$$

$$\partial_z \mathbf{v} - i(\gamma_D + \gamma) \mathbf{v} = 0 \quad z = a, \tag{2.10b}$$

$$P \mathbf{v} = \Psi(x, y) \quad z = g, \tag{2.10c}$$

where

$$P := \begin{pmatrix} 1 & 0 & 0 \\ 0 & 1 & 0 \\ \partial_x + i\alpha & \partial_y + i\beta & \partial_z - i\gamma \end{pmatrix}, \tag{2.10d}$$

and

$$\Psi := \begin{pmatrix} -A^1 - (\partial_x g)\{A^3 + v^3\} \\ -A^2 - (\partial_y g)\{A^3 + v^3\} \\ 0 \end{pmatrix}. \tag{2.10e}$$

We point out that while the divergence-free condition has become somewhat more involved, the dependence upon g in Ψ is now merely linear rather than exponential. The current can also be expressed in terms of the factored field by

$$J^1 = \frac{e^{i(\alpha x + \beta y - \gamma g(x,y))}}{ik} \left[-\partial_z v^1 + \partial_x v^3 + (i\gamma)v^1 + (i\alpha)v^3 - (\partial_y g) (\partial_x v^2 - \partial_y v^1 + (i\alpha)v^2 - (i\beta)v^1) \right], \tag{2.11a}$$

$$J^2 = \frac{e^{i(\alpha x + \beta y - \gamma g(x,y))}}{ik} \left[\partial_y v^3 - \partial_z v^2 + (i\beta)v^3 + (i\gamma)v^2 + (\partial_x g) (\partial_x v^2 - \partial_y v^1 + (i\alpha)v^2 - (i\beta)v^1) \right], \tag{2.11b}$$

$$J^3 = \frac{e^{i(\alpha x + \beta y - \gamma g(x,y))}}{ik} \left[(\partial_y g) (\partial_y v^3 - \partial_z v^2 + (i\beta)v^3 + (i\gamma)v^2) + (\partial_x g) (-\partial_z v^1 + \partial_x v^3 + (i\gamma)v^1 + (i\alpha)v^3) \right]. \tag{2.11c}$$

2.2 Change of Variables

As we have seen in previous publications [6–9] a well-chosen change of variables can have extremely beneficial effects for both the analysis and performance of Boundary Perturbation methods. As before we make the following “domain flattening” change of variables (the C-method in electromagnetics [2] or σ -coordinates in oceanography [13]):

$$x' = x, \quad y' = y, \quad z' = a \left(\frac{z - g}{a - g} \right). \tag{2.12}$$

Considering the new dependent variable

$$\mathbf{u}(x', y', z') := \mathbf{v} \left(x', y', \frac{(a - g)z'}{a} + g \right),$$

Equation (2.10) transforms to, upon dropping primes,

$$\Delta \mathbf{u} + 2i(\alpha, \beta, -\gamma) \cdot \nabla \mathbf{u} = \mathbf{F}(x, y, z; \mathbf{u}, g) \quad 0 < z < a, \tag{2.13a}$$

$$\partial_z \mathbf{u} - i(\gamma_D + \gamma) \mathbf{u} = \mathbf{R}(x, y; \mathbf{u}, g) \quad z = a, \tag{2.13b}$$

$$P \mathbf{u} = \mathbf{Q}(x, y; \mathbf{u}, g) \quad z = 0, \tag{2.13c}$$

where

$$\mathbf{F} = \partial_x \mathbf{F}_x + \partial_y \mathbf{F}_y + \partial_z \mathbf{F}_z + \mathbf{F}_h, \tag{2.13d}$$

$$\mathbf{F}_x = \frac{2}{a} g \partial_x \mathbf{u} + \frac{a - z}{a} (\partial_x g) \partial_z \mathbf{u} - \frac{1}{a^2} g^2 \partial_x \mathbf{u} - \frac{a - z}{a^2} g (\partial_x g) \partial_z \mathbf{u}, \tag{2.13e}$$

$$\mathbf{F}_y = \frac{2}{a} g \partial_y \mathbf{u} + \frac{a - z}{a} (\partial_y g) \partial_z \mathbf{u} - \frac{1}{a^2} g^2 \partial_y \mathbf{u} - \frac{a - z}{a^2} g (\partial_y g) \partial_z \mathbf{u}, \tag{2.13f}$$

$$\begin{aligned} \mathbf{F}_z &= \frac{a - z}{a} \{ (\partial_x g) \partial_x \mathbf{u} + (\partial_y g) \partial_y \mathbf{u} \} \\ &\quad - \frac{a - z}{a^2} \{ g (\partial_x g) \partial_x \mathbf{u} + g (\partial_y g) \partial_y \mathbf{u} \} \\ &\quad - \frac{(a - z)^2}{a^2} \{ (\partial_x g)^2 \partial_z \mathbf{u} + (\partial_y g)^2 \partial_z \mathbf{u} \}, \end{aligned} \tag{2.13g}$$

and

$$\begin{aligned} \mathbf{F}_h &= -\frac{1}{a} \{ (\partial_x g) \partial_x \mathbf{u} + (\partial_y g) \partial_y \mathbf{u} \} + \frac{1}{a^2} \{ g (\partial_x g) \partial_x \mathbf{u} + g (\partial_y g) \partial_y \mathbf{u} \} \\ &\quad + \frac{a - z}{a^2} \{ (\partial_x g)^2 \partial_z \mathbf{u} + (\partial_y g)^2 \partial_z \mathbf{u} \} + \frac{4i}{a} \{ \alpha g \partial_x \mathbf{u} + \beta g \partial_y \mathbf{u} \} \\ &\quad + \frac{2i(a - z)}{a} \{ \alpha (\partial_x g) \partial_z \mathbf{u} + \beta (\partial_y g) \partial_z \mathbf{u} \} - \frac{2i\gamma}{a} g \partial_z \mathbf{u} \\ &\quad - \frac{2i}{a^2} \{ \alpha g^2 \partial_x \mathbf{u} + \beta g^2 \partial_y \mathbf{u} \} \end{aligned}$$

$$-\frac{2i(a-z)}{a^2} \{ \alpha g(\partial_x g) \partial_z \mathbf{u} + \beta g(\partial_y g) \partial_z \mathbf{u} \}.$$

Furthermore, we have

$$\mathbf{R} = -\frac{1}{a} g i (\gamma_D + \gamma) \mathbf{u} \tag{2.13h}$$

and

$$\mathbf{Q} = \begin{pmatrix} -A^1 - (\partial_x g) \{A^3 + u^3\} \\ -A^2 - (\partial_y g) \{A^3 + u^3\} \\ Q^3 \end{pmatrix}, \tag{2.13i}$$

where

$$Q^3 = -\frac{1}{a} (i\gamma) g u^3 + \frac{1}{a} g \partial_x u^1 + (\partial_x g) \partial_z u^1 + \frac{i\alpha}{a} g u^1 + \frac{1}{a} g \partial_y u^2 + (\partial_y g) \partial_z u^2 + \frac{i\beta}{a} g u^2. \tag{2.13j}$$

The surface current, (2.8), can also be expressed in the new coordinates, but in the interest of brevity we suppress the details.

2.3 Transformed Field Expansions

Using the methods outlined in the previous work of the authors [7, 9], it can be shown that, if the boundary deformation is written $g = \varepsilon f$ and f is sufficiently smooth, then the transformed factored field \mathbf{u} (and the transformed current) depend analytically upon the parameter ε , i.e., the series

$$\mathbf{u} = \mathbf{u}(x, y, z; \varepsilon) = \sum_{n=0}^{\infty} \mathbf{u}_n(x, y, z) \varepsilon^n \tag{2.14}$$

converges *strongly* in an appropriate function space for ε sufficiently small. Depending on the smoothness of f this also implies analyticity of the original factored field, \mathbf{v} , and field, \mathbf{E} ; in particular, if f is real analytic then \mathbf{u} , \mathbf{v} and \mathbf{E} are all *jointly* analytic with respect to *all* variables.

These results suggest that a numerical procedure based upon the Boundary Perturbation expansion (2.14) coupled to a high-order spectral discretization of the \mathbf{u}_n (Fourier collocation in the x and y variables, and Chebyshev tau in the z variable) should be robust and highly accurate. For solutions of Laplace’s equation [7], the scalar Helmholtz equation [9], and the classical water wave problem [10] this “Transformed Field Expansion” (TFE) method has indeed displayed these properties. In this work we present this method as applied to the full vector electromagnetic Maxwell equations in three dimensions for the first time.

While many of the details of this TFE implementation are familiar from our previous work, there are some new considerations which we highlight below. To begin, the expansion (2.14) is inserted into (2.13) and, equating at perturbation order n , one finds the following problems to solve:

$$\Delta \mathbf{u}_n + 2i(\alpha, \beta, -\gamma) \cdot \nabla \mathbf{u}_n = \mathbf{F}_n(x, y, z) \quad 0 < z < a, \tag{2.15a}$$

$$\partial_z \mathbf{u}_n - i(\gamma_D + \gamma) \mathbf{u}_n = \mathbf{R}_n(x, y) \quad z = a, \quad (2.15b)$$

$$P \mathbf{u}_n = \mathbf{Q}_n(x, y) \quad z = 0, \quad (2.15c)$$

where the forms for \mathbf{F}_n and \mathbf{R}_n are easily deduced from our previous work (see, e.g., [6, 9]). The form for \mathbf{Q}_n requires some comment as, in our previous work, this term always corresponded to a simple Dirichlet condition which is trivially implemented. Here, the first two boundary conditions at $z = 0$ are, again, essentially Dirichlet conditions:

$$u_n^1 = \delta_{n,0}(-A^1) + \delta_{n,1}(-A^3(\partial_x f)) - (\partial_x f)u_{n-1}^3,$$

$$u_n^2 = \delta_{n,0}(-A^2) + \delta_{n,1}(-A^3(\partial_y f)) - (\partial_y f)u_{n-1}^3,$$

however, the final condition reads

$$(\partial_x + i\alpha)u_n^1 + (\partial_y + i\beta)u_n^2 + (\partial_z - i\gamma)u_n^3 = Q_n^3, \quad (2.16)$$

where

$$\begin{aligned} Q_n^3 = & -\frac{1}{a}(i\gamma)f u_{n-1}^3 + \frac{1}{a}f \partial_x u_{n-1}^1 + (\partial_x f)\partial_z u_{n-1}^1 + \frac{i\alpha}{a}f u_{n-1}^1 \\ & + \frac{1}{a}f \partial_y u_{n-1}^2 + (\partial_y f)\partial_z u_{n-1}^2 + \frac{i\beta}{a}f u_{n-1}^2. \end{aligned}$$

It would appear that the coupling in this last condition would entail significant complications in our numerical procedures, namely that the scalar Helmholtz solvers we devised in [9] would be inapplicable and a new *vector* solver would be necessary. However, closer inspection reveals that if u_n^1 and u_n^2 are found from their *uncoupled* equations, these functions can then be placed among the known quantities on the right-hand side of (2.16):

$$(\partial_z - i\gamma)u_n^3 = Q_n^3 - (\partial_x + i\alpha)u_n^1 - (\partial_y + i\beta)u_n^2.$$

Thus, the only (nontrivial) modification to our previous solution procedures is the accommodation of a Robin boundary condition in the solution of u_n^3 . All of this has been implemented and verified by comparison to solutions of the “Field Expansions” (Variation of Boundaries) algorithm of Bruno and Reitich [1] also designed for these biperiodic grating scattering configurations (see Table 2).

2.4 Families of Gratings

In addition to presenting, for the first time, the specification of a TFE algorithm for the full vector electromagnetic grating scattering problem, we can also describe a TFE algorithm for *families* of gratings akin to that found in [6]. In many engineering applications, gratings of interest are not shaped by isolated (biperiodic) functions, but rather come in families. For example, in the study of water waves (gravity waves on the surface of an ideal fluid of depth h which model open-ocean movements [5]) it is known that the shape, η , of traveling waves depend analytically upon a height/slope parameter, ε :

$$\eta = \eta(x, y; \varepsilon) = \sum_{n=0}^{\infty} \eta_n(x, y) \varepsilon^n, \quad (2.17)$$

cf. [10, 14]. The choice of ε for the name of the analyticity parameter is not accidental as we have found that by identifying this perturbation parameter with the one which appears in the expansion (2.14) in Sect. 2.3 yields an algorithm which has *greatly* advantaged computational complexity over state-of-the-art scattering solvers when anything more than a moderate sampling of grating profiles from the family is considered.

This TFE method for families of gratings simply amounts to the insertion of (2.17) into the transformed and phase extracted vector Helmholtz equations (2.13). In this regard we point out the crucial importance of both transformations we made: First, the phase extraction removes all terms of the form

$$e^{i(\alpha x + \beta y - \gamma \eta(x, y; \varepsilon))}$$

which would involve the expansion of the *composition* of two analytic functions, the exponential and η . Second, the change of independent variables (2.12) moves the shape of the grating from the domain definition to the right-hand-side of the vector Helmholtz problem on a *separable* domain. All of this permits an expansion of the transformed, phase extracted field \mathbf{u} into a Taylor series (cf. (2.14)) with terms at order n satisfying (2.15). Of course the specific *forms* of \mathbf{F}_n , \mathbf{Q}_n , and \mathbf{R}_n are somewhat different, but those of the former two have been presented in [6] while the latter are

$$Q_n^1 = \delta_{n,0}(-A^1) - A^3(\partial_x \eta_n) - \sum_{l=0}^n (\partial_x \eta_{n-l}) u_l^3,$$

$$Q_n^2 = \delta_{n,0}(-A^2) - A^3(\partial_y \eta_n) - \sum_{l=0}^n (\partial_y \eta_{n-l}) u_l^3,$$

and

$$Q_n^3 = -\frac{1}{a}(i\gamma) \sum_{l=0}^n \eta_{n-l} u_l^3 + \frac{1}{a} \sum_{l=0}^n \eta_{n-l} \partial_x u_l^1 + \sum_{l=0}^n (\partial_x \eta_{n-l}) \partial_z u_l^1$$

$$+ \frac{i\alpha}{a} \sum_{l=0}^n \eta_{n-l} u_l^1 + \frac{1}{a} \sum_{l=0}^n \eta_{n-l} \partial_y u_l^2$$

$$+ \sum_{l=0}^n (\partial_y \eta_{n-l}) \partial_z u_l^2 + \frac{i\beta}{a} \sum_{l=0}^n \eta_{n-l} u_l^2.$$

3 Numerical Results

We now describe numerical results which not only verify the accuracy and stability of our new algorithm for computing vector electromagnetic scattering from families of gratings, but also display the capabilities of our new approach. We note that these latter results contain the scattering information of hundreds to thousands of grating profiles, a collection of computations which would be well beyond the scope of even state-of-the-art electromagnetic solvers [15].

3.1 Verification

As we stated earlier, our numerical scheme is a Fourier collocation/Chebyshev tau/Taylor method which seeks to approximate the phase extracted, transformed field \mathbf{u} by

$$\mathbf{u}^{(N, N_1, N_2, N_y)}(x, y, z; \varepsilon) := \sum_{n=0}^N \sum_{p=-N_1/2}^{N_1/2-1} \sum_{q=-N_2/2}^{N_2/2-1} \sum_{l=0}^{N_y} \hat{\mathbf{u}}_n^{p,q,l} T_l \left(\frac{2z-a}{a} \right) \times \exp(i[(2\pi p/d_1)x + (2\pi q/d_2)y])\varepsilon^n,$$

where T_l is the l -th Chebyshev polynomial. Upon insertion of this form into (2.13) we are faced, at every perturbation order n and every wavenumber (p, q) , with the solution of a two-point boundary value problem in the z -variable via the Chebyshev tau method; for this we use the classical scheme of Gottlieb & Orszag [3] (Chap. 10). As in our related work, the question of the summation of the terms in the Taylor series in ε can be answered in (at least) two ways: Taylor summation or Padé approximation. It has been our consistent experience that Padé summation typically produces greatly enhanced numerical results (see, e.g., [7, 9]) and we again utilize this procedure in this work.

For completeness we recall the complexity estimates we made in [6] using this procedure for computing the scattering returns from Q profiles:

$$\mathcal{O}(N^2 N_1 \log(N_1) N_2 \log(N_2) N_y \log(N_y) + Q N N_1 N_2).$$

This is to be compared with the cost of a preconditioned iterative solver applied to an integral equation formulation accelerated, e.g., by the Fast Multipole Method [4] which is

$$\mathcal{O}(Q N_{iter} N_1 \log(N_1) N_2 \log(N_2)),$$

where N_{iter} is the number of iterations required for convergence. The cost of repeated integral equation solves will dominate that of our new approach roughly when

$$Q > N_y \log(N_y) \max \left\{ 1, \frac{N^2}{N_{iter}} \right\}$$

thus indicating the domain of utility of the method we advocate.

The terms in the expansion of the water wave surface (2.17) were computed using the stable, high-fidelity TFE procedure outlined in [10]. For this verification we selected the physical parameters $\tilde{g} = 1$ and $h = \infty$ corresponding to nondimensionalized gravity waves on deep water. Additionally, the traveling wave is periodic with respect to the cell

$$C_\theta := \left[\frac{2\pi}{\sin(\theta)}, 0 \right] \times \left[0, \frac{2\pi}{\cos(\theta)} \right] \tag{3.1}$$

and we initially choose $\theta = 45^\circ$, corresponding to surface waves periodic with respect to the square

$$[(2\pi)/\sin(\pi/4), 0] \times [0, (2\pi)/\cos(\pi/4)] \approx [8.88577, 0] \times [0, 8.88577].$$

The numerical parameters were set to $a = 0.1$, $N_1 = N_2 = 64$, $N_y = 48$ and $N = 30$. In Table 1 we present convergence results of our new scheme for families of gratings as compared to an “exact” solution provided by the TFE algorithm of Sect. 2.3. For this study we observe

Table 1 Relative error, measured in the L^∞ norm (cf. (3.2)), of the new TFE method for families of profiles as compared to the TFE method for a single profile ($N_1 = N_2 = 64$, $N_y = 48$, $N = 30$) for $(\alpha, \beta, \gamma) = (0, 0, 1.1)$ and $\mathbf{A} = (1, 0, 0)$

N	e_1	e_2	e_3
0	0.012715271	1.2722346	1.2721962
1	0.00011386439	0.0030028758	0.012870532
2	1.2427435×10^{-6}	7.0672938×10^{-5}	0.00012321859
3	1.0389127×10^{-8}	4.8027358×10^{-7}	1.3570777×10^{-6}
4	9.408323×10^{-11}	4.5756359×10^{-9}	1.1674027×10^{-8}
5	$5.1907967 \times 10^{-13}$	$3.1421886 \times 10^{-11}$	$8.7157665 \times 10^{-11}$
6	$7.1386884 \times 10^{-15}$	$2.9392388 \times 10^{-13}$	$1.0113276 \times 10^{-12}$
7	$2.8061017 \times 10^{-15}$	$9.7625387 \times 10^{-15}$	$1.1102099 \times 10^{-14}$
8	$2.8067652 \times 10^{-15}$	9.762775×10^{-15}	$6.2440711 \times 10^{-15}$

Table 2 Relative error, measured in the L^∞ norm (cf. (3.2)), of the new TFE method for families of profiles as compared to the FE method for a single profile ($N_1 = N_2 = 64$, $N = 30$) for $(\alpha, \beta, \gamma) = (0, 0, 1.1)$ and $\mathbf{A} = (1, 0, 0)$

N	e_1	e_2	e_3
0	0.012715271	1.2722346	1.2721962
1	0.00011386439	0.0030028758	0.012870532
2	1.2427435×10^{-6}	7.0672935×10^{-5}	0.00012321858
3	1.0386806×10^{-8}	4.8027368×10^{-7}	1.3570777×10^{-6}
4	$9.4396691 \times 10^{-11}$	4.5768494×10^{-9}	1.1674296×10^{-8}
5	$5.6871914 \times 10^{-12}$	$3.1498015 \times 10^{-11}$	$8.7194381 \times 10^{-11}$
6	$5.6077646 \times 10^{-12}$	$3.6194502 \times 10^{-12}$	$7.5191228 \times 10^{-12}$
7	$5.6077336 \times 10^{-12}$	$3.5664949 \times 10^{-12}$	$7.1365016 \times 10^{-12}$
8	$5.6077109 \times 10^{-12}$	$3.5664951 \times 10^{-12}$	7.136503×10^{-12}

the rapid convergence of our new method via the error measure of the j -th component of the current

$$e_j := \frac{|J^{j,N} - J^{j,exact}|}{|J^{j,exact}|} \tag{3.2}$$

where

$$J^{j,N}(x, y) := \sum_{n=0}^N J_n^j(x, y) \varepsilon^n,$$

as the perturbation order N is increased. To further verify our algorithm, we have also computed the “exact” solution via the Field Expansions approach of Bruno and Reitch [1] and report, in Table 2, the results of this comparison. We note the nearly identical behavior as observed in Table 1, though the sub-optimal accuracy as compared with these FE solutions is due to the limited resolution of both the classical TFE and our new TFE approaches in the z -direction.

3.2 Calculation of Efficiencies

Quantities of great engineering interest in the study of gratings are the scattering efficiencies [12]. Given the Rayleigh series representation of the scattered field as

$$\mathbf{E}(x, y, z) = \sum_{p=-\infty}^{\infty} \sum_{q=-\infty}^{\infty} \mathbf{D}_{p,q} e^{i(\alpha_p x + \beta_q y + i\gamma_{p,q} z)},$$

the efficiencies are defined as

$$e_{p,q} := \frac{|\mathbf{D}_{p,q}|^2 \gamma_{p,q}}{|\mathbf{A}|^2 \gamma_{0,0}}$$

for any $(p, q) \in U$, the set of propagating frequencies. With this definition in hand it is clear why these efficiencies are of such interest as they quantify the “energy fraction” in each mode which propagates away from the grating. We note for future reference that, for a lossless grating, there is a principle of conservation of energy which states that

$$\sum_{(p,q) \in U} e_{p,q} = 1,$$

so that the quantity

$$\delta = \left| 1 - \sum_{(p,q) \in U} e_{p,q} \right|, \tag{3.3}$$

is an “energy defect” and can be used as a diagnostic of convergence.

In Fig. 1 we plot the results of our computations for the efficiencies $e_{0,0}$ and $e_{1,1}$ as a function of the wave/height parameter ε . Here the water wave is on an ocean of depth $h = \infty$, gravity is scaled to $\tilde{g} = 1$, and the wave is periodic with respect to the cell C_{45° . The electromagnetic wave has frequency $(\alpha, \beta, \gamma) = (0, 0, 1.1)$ and the incident radiation has amplitude $\mathbf{A} = (1, 0, 0)$. The numerical parameters are $N_1 = N_2 = 64$, $N_y = 48$, and $N = 30$ for the simulation of both the traveling water wave and the electromagnetic scattering. The

Fig. 1 Plot of efficiencies $e_{0,0}$ and $e_{1,1}$ versus ε for an ocean of depth $h = \infty$ and radiation frequency $(\alpha, \beta, \gamma) = (0, 0, 1.1)$. The traveling ocean wave is periodic with respect to the cell C_θ , cf. (3.1), with $\theta = 45^\circ$ and the numerical parameters are $N_1 = N_2 = 64$, $N_y = 48$, and $N = 30$

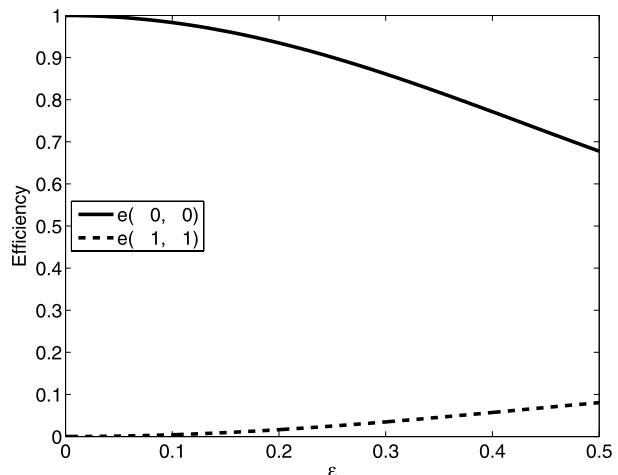


Fig. 2 Plot of energy defect, cf. (3.3), versus ε for an ocean of depth $h = \infty$ and radiation frequency $(\alpha, \beta, \gamma) = (0, 0, 1.1)$. The traveling ocean wave is periodic with respect to the cell C_θ , cf. (3.1), with $\theta = 45^\circ$ and the numerical parameters are $N_1 = N_2 = 64$, $N_y = 48$, and $N = 30$

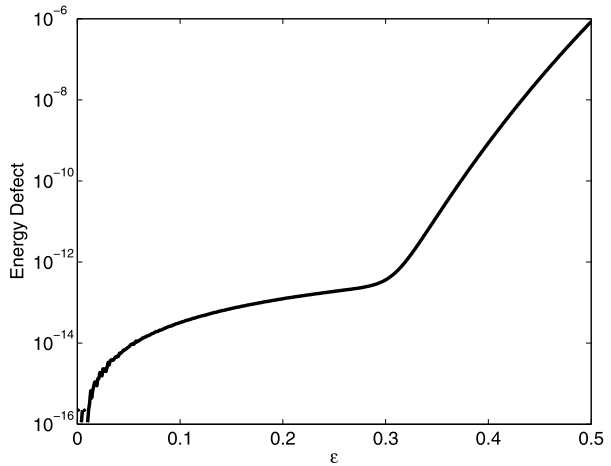
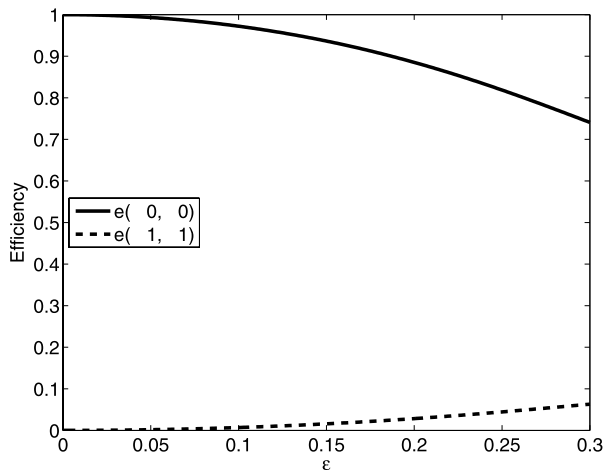


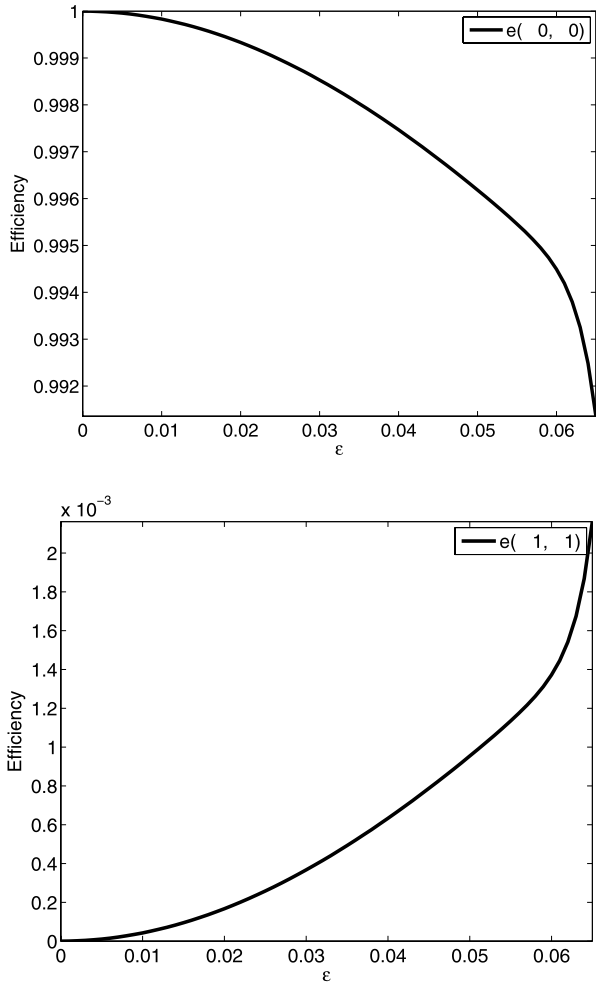
Fig. 3 Plot of efficiencies $e_{0,0}$ and $e_{1,1}$ versus ε for an ocean of depth $h = \infty$ and radiation frequency $(\alpha, \beta, \gamma) = (0, 0, 1.1)$. The traveling ocean wave is periodic with respect to the cell C_θ , cf. (3.1), with $\theta = 75^\circ$ and the numerical parameters are $N_1 = N_2 = 64$, $N_y = 48$, and $N = 30$



range of ε is chosen so that the energy defect δ , (3.3), is always less than 10^{-6} ; we make this claim quite precise in Fig. 2 which displays δ for this entire range of ε . We point out that the spacing in ε is set to $\Delta\varepsilon = 10^{-3}$ so that this plot actually displays the efficiency evaluated at 500 values of ε . While this would be prohibitively expensive for other solvers working one profile at a time, the additional cost for our algorithm to refine this sampling by a factor, say, of 10 or even 100 would be negligible.

In Fig. 3 we again plot the results of our computations for the efficiencies $e_{0,0}$ and $e_{1,1}$ as a function of the wave/height parameter ε . Here the water wave is parametrized by $h = \infty$ and $\tilde{g} = 1$ while being periodic with respect to the cell C_{75° . Again, the electromagnetic wave has frequency $(\alpha, \beta, \gamma) = (0, 0, 1.1)$ and the incident radiation has amplitude $\mathbf{A} = (1, 0, 0)$. The numerical parameters are $N_1 = N_2 = 64$, $N_y = 48$, and $N = 30$ for the simulation of both the traveling water wave and the electromagnetic scattering; the energy defect is always less than 10^{-6} . Once again, the spacing in ε is set to $\Delta\varepsilon = 10^{-3}$ so that the plot shows 300 values of the efficiencies.

Fig. 4 Plot of efficiencies $e_{0,0}$ and $e_{1,1}$ versus ε for an ocean of depth $h = 1/2$ and radiation frequency $(\alpha, \beta, \gamma) = (0, 0, 1.1)$. The traveling ocean wave is periodic with respect to the cell C_θ , cf. (3.1), with $\theta = 45^\circ$ and the numerical parameters are $N_1 = N_2 = 64$, $N_y = 48$, and $N = 30$

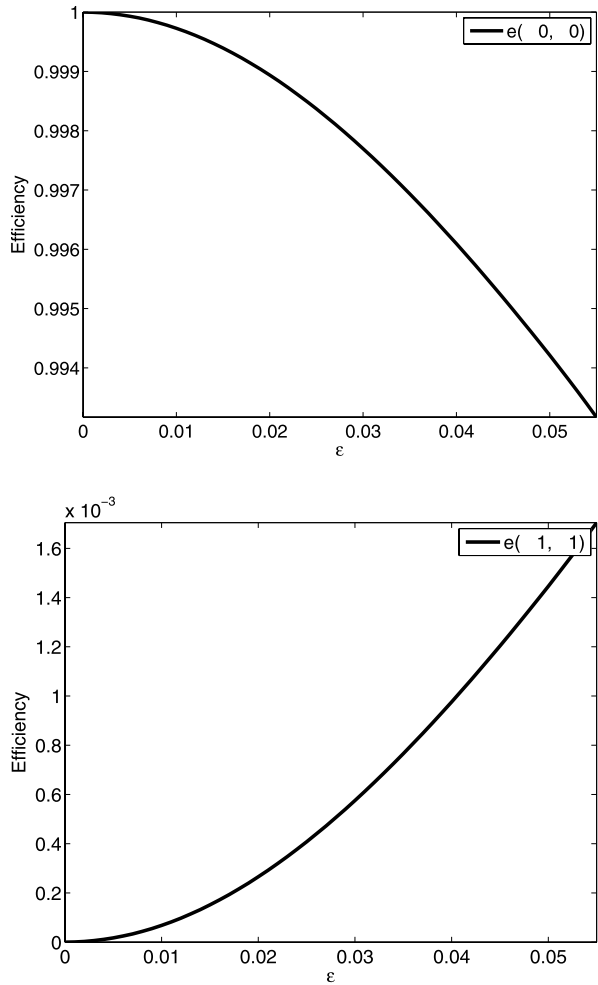


We conclude with the results depicted in Figs. 4 and 5, again focusing on the efficiencies $e_{0,0}$ and $e_{1,1}$. Now the water waves are on an ocean of depth $h = 1/2$ (fully within the “shallow water” regime) with $\tilde{g} = 1$. In Fig. 4 we have set $\theta = 45^\circ$, while in Fig. 5, $\theta = 75^\circ$. For consistency we have once again set $(\alpha, \beta, \gamma) = (0, 0, 1.1)$ and $\mathbf{A} = (1, 0, 0)$. The numerical parameters are $N_1 = N_2 = 64$, $N_y = 48$, and $N = 30$ for the simulation of both the traveling water wave and the electromagnetic scattering; again the energy defect is less than 10^{-6} . With the spacing $\Delta\varepsilon = 10^{-3}$ Fig. 4 represents 65 values of the efficiency, while Fig. 5 depicts 55 data points.

4 Conclusion

In this paper we have outlined a new method for computing three dimensional vector electromagnetic scattering returns by crossed gratings which is particularly efficient when the

Fig. 5 Plot of efficiencies $e_{0,0}$ and $e_{1,1}$ versus ε for an ocean of depth $h = 1/2$ and radiation frequency $(\alpha, \beta, \gamma) = (0, 0, 1.1)$. The traveling ocean wave is periodic with respect to the cell C_θ , cf. (3.1), with $\theta = 75^\circ$ and the numerical parameters are $N_1 = N_2 = 64$, $N_y = 48$, and $N = 30$



gratings come in parametrized families. The method is an extension of the authors’ previous work on similar calculations for the scalar Helmholtz equation in two dimensions. The details for overcoming the algorithmic complications of not only the additional spatial dimension but also the vector character of the governing equations are presented. The results of several numerical experiments to verify our scheme and display its capabilities are also shown.

5 Dedication

I (D.P.N.) was a student of David Gottlieb in graduate school at Brown University’s Division of Applied Mathematics, and was profoundly influenced not only by his mathematics but also by his personal character. By the fact that nearly all of my publications feature Professor Gottlieb’s high-order spectral methods (together with a citation to his seminal 1977 work with S. Orszag, *Numerical Analysis of Spectral Methods: Theory and Applications* [3]), it

is clear that I consider them to be both the most elegant and, quite often, the most efficient means of solving a differential equation numerically. Though I was not supervised by David, his ideas and influence are clearly stamped on both my thesis and the remainder of my published work. Of equal, and perhaps greater, value for me was the example he set as a devoted husband, father, grandfather, and friend. It was truly remarkable to see such a distinguished academic figure so deeply rooted in his family, and it is something I will never forget.

Acknowledgement DPN gratefully acknowledges support from the NSF through grant DMS-0810958.

References

1. Bruno, O.P., Reitich, F.: Numerical solution of diffraction problems: A method of variation of boundaries. III. Doubly periodic gratings. *J. Opt. Soc. Am. A* **10**(12), 2551–2562 (1993)
2. Chandezon, J., Maystre, D., Raoult, G.: A new theoretical method for diffraction gratings and its numerical application. *J. Opt.* **11**(7), 235–241 (1980)
3. Gottlieb, D., Orszag, S.A.: *Numerical Analysis of Spectral Methods: Theory and Applications*. CBMS-NSF Regional Conference Series in Applied Mathematics, vol. 26. Society for Industrial and Applied Mathematics, Philadelphia (1977)
4. Greengard, L., Rokhlin, V.: A fast algorithm for particle simulations. *J. Comput. Phys.* **73**(2), 325–348 (1987)
5. Lamb, H.: *Hydrodynamics*, 6th edn. Cambridge University Press, Cambridge (1993)
6. Nicholls D.P.: A rapid boundary perturbation algorithm for scattering by families of rough surfaces. *J. Comput. Phys.* **228**(9), 3405–3420 (2009)
7. Nicholls, D.P., Reitich, F.: Stability of high-order perturbative methods for the computation of Dirichlet-Neumann operators. *J. Comput. Phys.* **170**(1), 276–298 (2001)
8. Nicholls, D.P., Reitich, F.: Shape deformations in rough surface scattering: Cancellations, conditioning, and convergence. *J. Opt. Soc. Am. A* **21**(4), 590–605 (2004)
9. Nicholls, D.P., Reitich, F.: Shape deformations in rough surface scattering: Improved algorithms. *J. Opt. Soc. Am. A* **21**(4), 606–621 (2004)
10. Nicholls, D.P., Reitich, F.: Rapid, stable, high-order computation of traveling water waves in three dimensions. *Eur. J. Mech. B, Fluids* **25**(4), 406–424 (2006)
11. Nicholls, D.P., Reitich, F.: Boundary perturbation methods for high-frequency acoustic scattering: Shallow periodic gratings. *J. Acoust. Soc. Am.* **123**(5), 2531–2541 (2008)
12. Petit, R. (ed.): *Electromagnetic Theory of Gratings*. Springer, Berlin (1980)
13. Phillips, N.A.: A coordinate system having some special advantages for numerical forecasting. *J. Atmos. Sci.* **14**(2), 184–185 (1957)
14. Reeder, J., Shinbrot, M.: Three dimensional nonlinear wave interaction in water of constant depth. *Nonlinear Anal.* **5**, 303–323 (1981)
15. Reitich, F., Tamma, K.: State-of-the-art, trends, and directions in computational electromagnetics. *CMES Comput. Model. Eng. Sci.* **5**(4), 287–294 (2004)